PHYSICAL REVIEW B **82**, 020403(R) (2010)

Tilted elliptical Dirac cones at a half-metal surface

Stephen J. Jenkins
Department of Chemistry, University of Cambridge, Lensfield Road, Cambridge CB2 1EW, United Kingdom
(Received 4 May 2010; published 16 July 2010)

The surface electronic structure of the half-metallic alloy NiMnSb is investigated in detail, revealing the presence of Dirac cones in the minority-spin states. Surface-localized carriers of suitable energy will consequently behave as massless Dirac fermions, a remarkable situation for a half-metallic material and potentially of great significance in future spintronic device applications. Unlike related features observed previously in graphene and at the surfaces of topological insulators, the Dirac cones described here are of elliptical cross section and are tilted with respect to the energy axis. Such unique properties are permitted due to the lower symmetry in the present case.

DOI: 10.1103/PhysRevB.82.020403 PACS number(s): 75.70.Rf, 73.20.At, 71.10.Pm, 73.22.Pr

Recent years have witnessed considerable excitement over the experimental realization of graphene,[1] a material whose electronic band structure includes characteristic conical features at high-symmetry points within the Brillouin zone.[2] Similar exotic features have also been observed in the surface electronic structure of so-called topological insulators.[3–15] In either case, electrons in the vicinity of a cone exhibit linear dispersion and are expected to behave as massless Dirac fermions confined within a two-dimensional plane. The consequences of this unusual property for electronic-transport phenomena are inevitably rather profound. Here, we demonstrate the existence of a third class of material in which Dirac cones may be found, by analyzing in detail the surface- and interface-localized states of NiMnSb, a half-metallic semi-Heusler alloy. In contrast to examples noted previously in graphene and the topological insulators, the cones in the present case are tilted with respect to the energy axis, and are of elliptical cross section.

Half-metals are ferromagnetic materials in which electrons of one spin orientation inhabit a metallic band structure while those of the opposing spin inhabit an insulating one. Several candidate half-metallic materials have been identified by theory to date, including various oxides, perovskites, and pnictides. The concept was originally developed, however, in the context of the semi-Heusler alloy NiMnSb, predicted to be half-metallic by de Groot *et al.*[16] in 1983. In relation to the potential exploitation of half metals for spin injection into nonmagnetic materials, the present author has previously published theoretical analyses of surface- and interface-localized minority-spin states predicted for NiMnSb{001}[17] and NiMnSb{001}/Sb,[18] in which the presence of "a form of conical intersection"[17] in the electronic band structure was inferred but regrettably not explored. In view of subsequent developments, this feature deserves now to be properly characterized and discussed in detail. To that end, our first-principles density functional theory (DFT) calculations have been extended to extract the key parameters of the surface electronic structure.[19]

The zone-center minority-spin surface states of clean MnSb-terminated NiMnSb{001} have previously been identified at 0.20 and 0.44 eV above the Fermi level, with A_1 and B_1 symmetries, respectively;[17] these symmetry classifications are retained for all wave vectors parallel to the $\mathbf{b_1}$ or $\mathbf{b_2}$ reciprocal lattice vectors (which one should note are crystallographically inequivalent for this material). Traversing the $\mathbf{b_2}$ axis from the $\bar{\Gamma}$ point, the state with B_1 symmetry disperses upward and that with A_1 symmetry downward while the reverse is true along the $\mathbf{b_1}$ axis. Since the orthogonality of these states is guaranteed by symmetry, the latter fact implies a band crossing must occur at two points situated either side of the zone center on the $\mathbf{b_1}$ axis; in our calculations, these crossings occur at $\mathbf{k_0}=(\pm 0.087, 0.000)$ with energy $E_0=0.31$ eV relative to the Fermi level.[20] The minority-spin surface bands in the vicinity of the band-crossing points therefore take the form of a cone within the three-dimensional space spanned by the energy and the two-dimensional wave vector. Far from the apex of either cone, the structure revealed by our new calculations is necessarily more complicated (see Fig. 1) but the conical approximation holds rather well for energies within about 0.1 eV of E_0.

In contrast to the Dirac cones calculated for graphene and the topological insulators, which are effectively isotropic sufficiently close to their apices,[21] the conical structures found here are tilted somewhat; moreover, the cross section of each cone, taken perpendicular to its principal axis, is now seen to be elliptical rather than circular. These deviations from the ideality of an upright circular cone are permitted because the apices in the present case are located at positions of rather lower symmetry than in those other systems.

For a wave vector $\mathbf{k}$ close to one of the "Dirac points," $\mathbf{k_0}$, we may conveniently define a relative wave vector $\mathbf{q}$, having components q_1 and q_2 parallel to the $\mathbf{b_1}$ and $\mathbf{b_2}$ reciprocal lattice vectors, respectively. Within such a frame of refer-

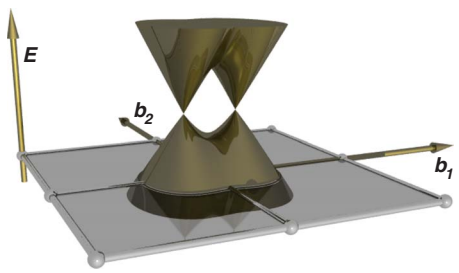

FIG. 1. (Color online) Minority-spin surface-state dispersion for clean NiMnSb{001}. The flat horizontal plane represents the Fermi level, and extends to fill the two-dimensional surface Brillouin zone; energy is represented on the vertical axis.

TABLE I. Parameters entering into Eq. (1) for both clean and Sb-covered NiMnSb{001}. The positive (negative) sign for A is associated with the cone having positive (negative) displacement along the $\mathbf{b_1}$ axis.

System	$\mathbf{k_0}$	E_0 (eV)	A (eV)	B (eV^2)	C (eV^2)
Clean	$(\pm 0.087, 0.000)$	0.31	± 0.479	5.129	8.535
Sb (1 ML)	$(\pm 0.114, 0.000)$	0.24	± 1.555	5.339	12.467
Sb (2 ML)	$(\pm 0.135, 0.000)$	0.18	± 1.195	5.295	9.492
Sb (3 ML)	$(\pm 0.126, 0.000)$	0.21	± 0.786	6.478	8.255

ence, the tilted conical structure is well represented close to the Dirac point by

$$(E - E_0)^2 + Aq_1(E - E_0) - Bq_1^2 - Cq_2^2 = 0, \tag{1}$$

where the energy E clearly reduces to E_0 at the cone apex but is double valued for all nonzero choices of $\mathbf{q}$. Note that an *upright* cone is obtained in the case where A vanishes, and that an upright *circular* cone is recovered in the case where A vanishes and $B=C$. The *actual* values of these constants may readily be determined by matching to the DFT-calculated behavior of the high- and low-energy solutions E^+ and E^- in certain special cases. Specifically, it may be shown that

$$A = -\left(\frac{\partial \bar{E}}{\partial q_1}\right)_{q_2=0}, \tag{2}$$

$$B = \frac{1}{4}\left[\left(\frac{\partial \bar{\bar{E}}}{\partial q_1}\right)^2_{q_2=0} - \left(\frac{\partial \bar{E}}{\partial q_1}\right)^2_{q_2=0}\right], \tag{3}$$

$$C = \left(\frac{\partial E^+}{\partial q_2}\right)^2_{q_1=0} = \left(\frac{\partial E^-}{\partial q_2}\right)^2_{q_1=0} \tag{4}$$

with $\bar{E}=E^+ + E^-$ and $\bar{\bar{E}}=E^+ - E^-$ introduced to aid clarity. Values of these parameters obtained for the clean NiMnSb{001} surface are collated in Table I.

Notwithstanding these deviations from the geometry of an upright circular cone the essential phenomenology of massless Dirac fermions will be retained, albeit with an implicit angular dependence to be incorporated into the effective speed of light. Specifically, the massless fermion solutions represented on the upper half of one of the cones at $\mathbf{k}=\mathbf{k_0}+\mathbf{q}$ are complemented by massless antifermion solutions on the lower half of the same cone at $\mathbf{k}=\mathbf{k_0}-\mathbf{q}$ (i.e., having relative wave vector $\mathbf{q}$ inverted with respect to $\mathbf{k_0}$). In the usual theoretical treatment, as applied typically to graphene, the eigenvalue associated with a suitably defined "helicity" operator changes sign between any given fermion solution and its antifermion counterpart with the inverted relative wave vector; by virtue of the massless status of these Dirac excitations, this helicity in fact corresponds to a well-defined "chirality" that is independent of the reference frame employed.[2] This symmetry, deriving from the conical nature of the dispersion, is additional to any other symmetries dictated by the crystal structure but becomes increasingly approximate with increasing distance from the Dirac point, as the conical approximation itself becomes progressively less appropriate. The combination of conical symmetry with the ordinary crystalline symmetry of the surface implies some quite remarkable features, as we now discuss.

Introducing $\mathbf{M}$ as the transformation matrix that effects a reflection across the $\mathbf{b_1}$ axis, let us begin by noting the degeneracy of fermion states with wave vectors $\mathbf{Mk}$ and $\mathbf{k}$,

$$E^+_{\mathbf{Mk}} = E^+_{\mathbf{k}}. \tag{5}$$

Moreover, we also note that the square moduli of the corresponding fermion eigenfunctions $|\mathbf{Mk}^+\rangle$ and $|\mathbf{k}^+\rangle$ are related by symmetry according to

$$|\mathbf{Mk}^+\rangle\langle\mathbf{Mk}^+| = \mathbf{M}|\mathbf{k}^+\rangle\langle\mathbf{k}^+|\mathbf{M} \tag{6}$$

with similar expressions for the antifermion solutions represented by energies $E^-_{\mathbf{Mk}}$ and $E^-_{\mathbf{k}}$ and by state vectors $|\mathbf{Mk}^-\rangle$ and $|\mathbf{k}^-\rangle$. These relationships are graphically illustrated in Fig. 2, where one may, for example, readily confirm that the square modulus of the fermion eigenfunction at $\mathbf{k}=(0.077, -0.010)$ is indeed the mirror image of the same function evaluated for the fermion solution at $\mathbf{k}=(0.077, 0.010)$. Similar relationships may also be discerned in respect of the antifermion solutions at the same pair of wave vectors and between the two fermion solutions (or two antifermion solutions) at $\mathbf{k}=(0.097, \pm 0.010)$. These are effectively statements about chirality in the chemical sense, albeit applied directly to orbitals rather than molecules, amounting to an assertion that electron-density distributions arising from states with wave vectors symmetrically located either side of a mirror plane are necessarily enantiomorphically related.

While the above symmetry relationships derive from the crystalline symmetry of the surface and are precise, we can also similarly represent the approximate symmetry relationships between fermion and antifermion states with relative wave vector $\mathbf{q}$ inverted across the Dirac cone. Thus, we have

$$E^+_{\mathbf{k_0}+\mathbf{q}} - E_0 \approx -(E^-_{\mathbf{k_0}-\mathbf{q}} - E_0) \tag{7}$$

and

$$|(\mathbf{k_0}+\mathbf{q})^+\rangle\langle(\mathbf{k_0}+\mathbf{q})^+| \approx |(\mathbf{k_0}-\mathbf{q})^-\rangle\langle(\mathbf{k_0}-\mathbf{q})^-| \tag{8}$$

for all sufficiently small values of $\mathbf{q}$, as again illustrated by Fig. 2 [e.g., the square modulus of the fermion eigenfunction at $\mathbf{k}=(0.077, 0.010)$ is identical to that of the antifermion eigenfunction at $\mathbf{k}=(0.097, -0.010)$]. These relationships are manifestations of chirality in the field theoretic sense.

Combining these two different symmetries, it is possible to predict an interesting special case. Defining $\{\mathbf{k_m}\}$ to be that subset of $\{\mathbf{k}=\mathbf{k_0}+\mathbf{q}\}$ for which $\mathbf{q}$ is both sufficiently small

and lies parallel to the $\mathbf{b_2}$ surface direction (i.e., $\mathbf{Mq}=-\mathbf{q}$) it is possible to show that

$$E^{+}_{\mathbf{k_m}} - E_0 \approx -(E^{-}_{\mathbf{k_m}} - E_0) \tag{9}$$

and

$$|\mathbf{k_m^+}\rangle\langle\mathbf{k_m^+}| \approx \mathbf{M}|\mathbf{k_m^-}\rangle\langle\mathbf{k_m^-}|\mathbf{M} \tag{10}$$

implying that although the fermion and antifermion solutions found at the *same* wave vector do *not* form a particle/antiparticle pair, nevertheless there *does* exist an approximate symmetry relationship (specifically, an enantiomorphic one) between their electron-density distributions. This can be clearly seen in Fig. 2 at either $\mathbf{k}=(0.087,0.010)$ or at $\mathbf{k}=(0.087,-0.010)$.

Finally, we turn to the question of stability. Dirac cones in graphene are quite susceptible to disruption by external perturbations, or indeed by the influence of spin-orbit coupling within an ostensibly perfect lattice. Here, in contrast, it seems unlikely that spin-orbit effects should play a significant role since there is no spin degeneracy in the conical feature to start with. As for the effect of external perturbation, there are strong grounds for believing the cones to be quite robust, based on their behavior upon deposition of Sb overlayers. As previously reported,[18] calculations involving one, two, or three complete monolayers of Sb indicate that the surface states of NiMnSb{001} evolve into interface-localized states that retain much of their original structure. In particular, the present reanalysis confirms that Dirac cones remain in evidence, albeit somewhat modified; their parameters are again collated in Table I.

In summary, it has been demonstrated that robust Dirac cones exist in the minority-spin surface states of half-metallic NiMnSb. In contrast to other reported instances in graphene and the topological insulators, these cones are elliptical in cross section, and tilted with respect to the energy axis. Nevertheless, their linear dispersion implies that charge carriers of suitable energy will behave as massless Dirac fermions/antifermions, as borne out by examination of the calculated eigenfunctions.

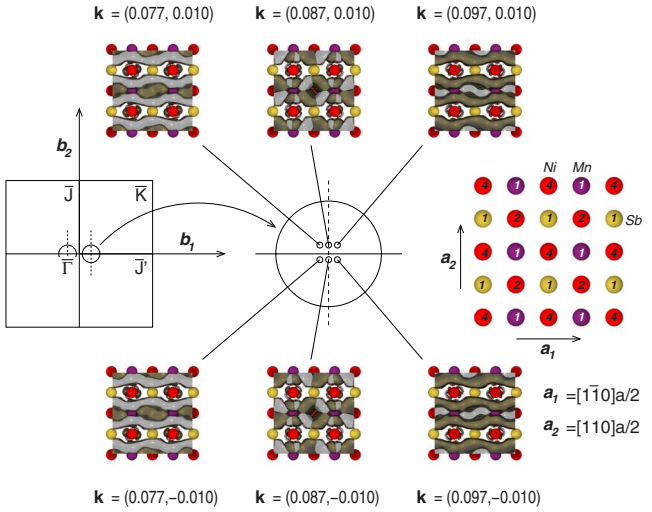

FIG. 2. (Color online) Minority-spin surface states in the vicinity of the Dirac point. The square modulus of the fermion eigenfunction (i.e., the solution found on the upper sheet of the cone) is depicted by a silver (light) isosurface while that corresponding to the antifermion eigenfunction (i.e., the solution found on the lower sheet of the cone) is depicted by a bronze (dark) isosurface. Note that for any given fermion solution the *corresponding* antifermion solution is to be found at the wavevector inverted across the Dirac point. Isosurfaces are drawn at a threshold density of 1.2×10^{-2} Å^{-3}. Also depicted are the Brillouin zone and a plan view of the surface labeled with numerals indicating the layer to which each visible atom belongs.

The author is grateful for support from The Royal Society.

[1] K. S. Novoselov, A. K. Geim, S. V. Morozov, D. Jiang, Y. Zhang, S. V. Dubonos, I. V. Grigorieva, and A. A. Firsov, Science **306**, 666 (2004).
[2] A. H. Castro Neto, F. Guinea, N. M. R. Peres, K. S. Novoselov, and A. K. Geim, Rev. Mod. Phys. **81**, 109 (2009).
[3] L. Fu, C. L. Kane, and E. J. Mele, Phys. Rev. Lett. **98**, 106803 (2007).
[4] L. Fu and C. L. Kane, Phys. Rev. B **76**, 045302 (2007).
[5] L. Fu and C. L. Kane, Phys. Rev. Lett. **100**, 096407 (2008).
[6] D. Hsieh, D. Qian, L. Wray, Y. Xia, Y. S. Hor, R. J. Cava, and M. Z. Hasan, Nature (London) **452**, 970 (2008).
[7] D. Hsieh *et al.*, Nature (London) **460**, 1101 (2009).
[8] D. Hsieh, Y. Xia, D. Qian, L. Wray, F. Meier, J. H. Dil, J. Osterwalder, L. Patthey, A. V. Fedorov, H. Lin, A. Bansil, D. Grauer, Y. S. Hor, R. J. Cava, and M. Z. Hasan, Phys. Rev. Lett. **103**, 146401 (2009).
[9] Y. Xia, D. Qian, D. Hsieh, L. Wray, A. Pal, H. Lin, A. Bansil, D. Grauer, Y. S. Hor, R. J. Cava, and M. Z. Hasan, Nat. Phys. **5**, 398 (2009).
[10] Y. S. Hor, A. Richardella, P. Roushan, Y. Xia, J. G. Checkelsky, A. Yazdani, M. Z. Hasan, N. P. Ong, and R. J. Cava, Phys. Rev. B **79**, 195208 (2009).
[11] Y. L. Chen *et al.*, Science **325**, 178 (2009).
[12] P. Roushan, J. Seo, C. V. Parker, Y. S. Hor, D. Hsieh, D. Qian, A. Richardella, M. Z. Hasan, R. J. Cava, and A. Yazdani, Nature (London) **460**, 1106 (2009).
[13] L. Fu, Phys. Rev. Lett. **103**, 266801 (2009).
[14] H. Z. Lu, W. Y. Shan, W. Yao, Q. Niu, and S. Q. Shen, Phys. Rev. B **81**, 115407 (2010).
[15] M. Hasan and C. Kane, arXiv:1002.3895, Rev. Mod. Phys. (to be published).
[16] R. A. de Groot, F. M. Mueller, P. G. van Engen, and K. H. J. Buschow, Phys. Rev. Lett. **50**, 2024 (1983).
[17] S. J. Jenkins and D. A. King, Surf. Sci. Lett. **494**, L793 (2001).
[18] S. J. Jenkins and D. A. King, Surf. Sci. Lett. **501**, L185 (2002).
[19] See supplementary material at http://link.aps.org/supplemental/10.1103/PhysRevB.82.020403 for fine points of the DFT methodology, together with tabulations of the calculated surface geometries obtained.
[20] Throughout this work, wave-vector components have been expressed as dimensionless fractions of the recpirocal lattice vectors $\mathbf{b_1}$ and $\mathbf{b_2}$, leading to the units quoted in Table I. Note that $|\mathbf{b_1}|=|\mathbf{b_2}|=1.51$ Å^{-1}.
[21] I. F. Herbut, Phys. Rev. B **79**, 193405 (2009).